Thermodynamic optimization of multi-stage cryogenic systems

C. S. Kirkconnell, and D. G. T. Curran

Citation: AIP Conference Proceedings **613**, 1123 (2002); doi: 10.1063/1.1472137
View online: https://doi.org/10.1063/1.1472137
View Table of Contents: http://aip.scitation.org/toc/apc/613/1
Published by the American Institute of Physics

HTML ABSTRACT + LINKS

THERMODYNAMIC OPTIMIZATION OF MULTI-STAGE CRYOGENIC SYSTEMS

C.S. Kirkconnell[1] and D.G.T. Curran[2]

[1]Irvine Sensors Corporation
Costa Mesa, California 92626

[2]The Aerospace Corporation
El Segundo, California 90009

ABSTRACT

Design point temperatures are relatively unconstrained for the warmer upper stage(s) of multi-stage cryogenic systems. For example, a sensor design in which an ambient temperature telescope is used to focus an image on an infrared focal plane array (IRFPA) might have only the operating temperature of the IRFPA as an operational requirement. With the advent of high capacity, multi-stage, long-life cryocoolers, thermodynamic optimization of the integrated system for maximum efficiency has become feasible. The proper thermodynamic optimization model includes both the thermal design of the system and the thermodynamic performance of the cryocooler(s) under consideration. In general, the optimum operating point for the total system is shown to lie between the optimum operating point of the selected cryocooler and the theoretical optimum of the system being cooled. Using Second Law techniques and typical physical characteristics for the thermal systems of interest, this paper presents a methodology for identifying the optimum thermodynamic operating point for the total system, which in turn yields the upper stage temperatures and the optimum cryocooler for the selected thermal configuration.

INTRODUCTION

Focusing solely on the cryocooler or the thermal design rather than the complete system can compromise the thermodynamic optimization of cryogenic systems. One of the key decisions related to the design of an efficient multi-stage system is the determination of the optimum operating temperatures for the upper stages. Consider a two-stage, actively cooled cryogenic system with a superconducting device at the second (coldest) stage and a heat intercept shield at the first (warmer) stage. The operating temperature of the second stage is determined by the requirement to operate at some fraction of the critical temperature of the device, T_c, but the selection of the first stage temperature is solely determined by the operating point that requires the least total cryocooler input power. This is a common scenario in which the coldest stage temperature is determined by the operating requirements of the device, but the selection of the upper stage temperature(s) is somewhat arbitrary. Consideration of temperature dependent properties of the structural supports and multi-layer insulation (MLI) blankets, heat generating sources, device dissipation, and heat

CP613, *Advances in Cryogenic Engineering: Proceedings of the Cryogenic Engineering Conference, Vol. 47,* edited by Susan Breon et al.
© 2002 American Institute of Physics 0-7354-0059-8/02/$19.00

transfer between temperature reservoirs must all be coupled with real-world cryocooler operating characteristics to determine the optimum first stage temperature. This paper presents a method for performing this type of thermodynamic design optimization based upon entropy generation, $\dot{S}_{gen}$, minimization techniques.

Modern efforts in the area of thermodynamic optimization through entropy generation minimization are largely due to the work of Bejan in the 1970s. This technique was used by Bejan and Smith to optimize structural supports for a liquid helium storage tank [1] and by Bejan in the optimization of heat exchanger design [2]. Hilal and Boom [3] and Seol, *et al.* [4] extended the work of Bejan and Smith on structural support optimization to consider discrete, rather than continuous, refrigeration along the length of the support. They approached the problem from the mathematically different but functionally equivalent viewpoint of refrigerator power minimization. Recently, Chang and Sciver [5] considered the analogous problem of the thermodynamic optimization of superconducting current leads with thermal intercepts.

THEORETICAL DEVELOPMENT OF GENERAL TWO STAGE MODEL

The methodology described herein is applicable to single-stage and multi-stage cryogenic systems; the entropy generation model for a two-stage system is presented here for the purpose of concept illustration. Consider the thermal system described in Figure 1. Cryogenic devices reside at the coldest and intermediate temperature reservoirs, T_L and T_M, and the electrical dissipations of the devices are $\dot{Q}_{g,L}$ and $\dot{Q}_{g,M}$, respectively. The total load at each stage is determined by the sum of the dissipative load and the net parasitic load. Parasitic loads are due to conductive, convective, and radiative heat transfer between temperature reservoirs. The first two modes are both characterized by linear expressions and are grouped together and denoted by the subscript "*lin*," and the radiative parasitic loads are labeled "*rad*." Note that for the general case, the 2nd stage is subject to parasitic loading from both the intermediate (T_M) and boundary (T_H) temperature reservoirs.

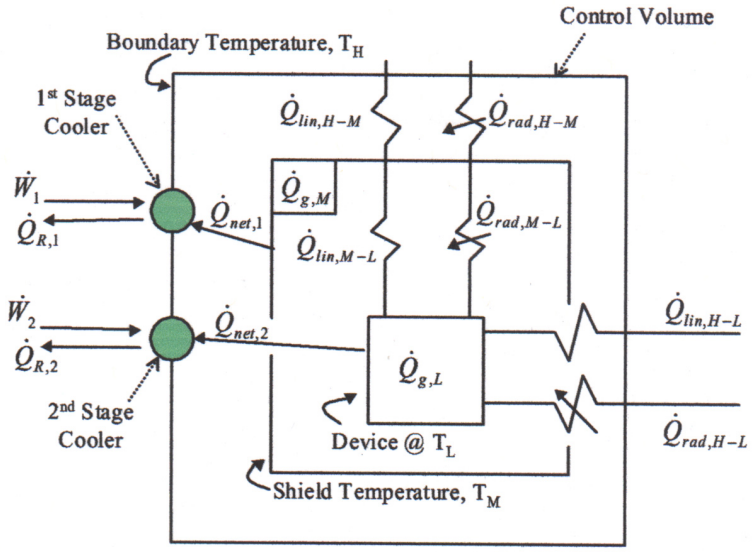

FIGURE 1. Thermal schematic of two-stage cryogenic system showing the intercept of a portion of the parasitic load at the intermediate temperature level.

The sum of the 2nd stage loads yields the net thermal load by the expression

$$\dot{Q}_{net,2} = \dot{Q}_{g,L} + \dot{Q}_{lin,M-L} + \dot{Q}_{rad,M-L} + \dot{Q}_{lin,H-L} + \dot{Q}_{rad,H-L}. \quad (1)$$

Similarly, the 1st stage net thermal load is given by

$$\dot{Q}_{net,1} = \dot{Q}_{g,M} + \dot{Q}_{lin,H-M} + \dot{Q}_{rad,H-M} - \dot{Q}_{lin,M-L} - \dot{Q}_{rad,M-L} \quad (2)$$

where the heat leak from the 1st stage to the 2nd stage is taken into account for system-level energy balance. For convenience, the parasitic loads are grouped as follows:

$$\dot{Q}_{p,HM} = \dot{Q}_{lin,H-M} + \dot{Q}_{rad,H-M}, \quad (3)$$

$$\dot{Q}_{p,HL} = \dot{Q}_{lin,H-L} + \dot{Q}_{rad,H-L}, \quad (4)$$

$$\dot{Q}_{p,ML} = \dot{Q}_{lin,M-L} + \dot{Q}_{rad,M-L}. \quad (5)$$

The net refrigeration required at each stage is equal to the corresponding net load, and the cryocooler input power required to deliver the specified refrigeration capacity is shown. Conservation of energy requires that the cryocooler heat rejection at each stage be equal to the input power plus the net refrigeration:

$$\dot{Q}_{R,1} = \dot{W}_1 + \dot{Q}_{net,1}, \text{ and} \quad (6)$$

$$\dot{Q}_{R,2} = \dot{W}_2 + \dot{Q}_{net,2}. \quad (7)$$

Note that this formulation is general with respect to the use of either a single two-stage cryocooler or two single-stage cryocoolers.

The general form of the entropy generation equation for a temperature-controlled, closed system with discrete heat transfer interactions comes from the time differentiation of Bejan's expression for a simple closed system [6]:

$$\dot{S}_{gen} = \frac{dS}{dt} - \sum_i \frac{\dot{Q}_i}{T_i}. \quad (8)$$

The time rate of change of entropy, S, is zero for steady state. Entropy generation equations can be written for the cryocooler, the subsystem being cooled, and the sum of the two, which is the total cryogenic system. For the cryocooler(s), the rate of entropy generation is defined by the expression

$$\dot{S}_{gen,cooler} = \frac{\dot{Q}_{R,1} + \dot{Q}_{R,2}}{T_H} - \frac{\dot{Q}_{p,HM} + \dot{Q}_{g,M} - \dot{Q}_{p,ML}}{T_M} - \frac{\dot{Q}_{p,HL} + \dot{Q}_{p,ML} + \dot{Q}_{g,L}}{T_L}. \quad (9)$$

Heat flows into the cryocooler are heat flows out of the subsystem being cooled, and this is reflected by the signs in the corresponding equation for the cooled subsystem:

$$\dot{S}_{gen,subsys} = \frac{\dot{Q}_{p,HM} + \dot{Q}_{g,M} - \dot{Q}_{p,ML}}{T_M} + \frac{\dot{Q}_{p,HL} + \dot{Q}_{p,ML} + \dot{Q}_{g,L}}{T_L} - \frac{\dot{Q}_{p,HM} + \dot{Q}_{p,HL}}{T_H}. \quad (10)$$

The parasitic heat leak from the intermediate temperature to the low temperature manifests itself as a decrease in the entropy generation in the first stage and an increase in the entropy generation in the second stage, and the result is a net increase in the entropy generation. The electrical dissipation loads result in entropy generation at the respective temperature

reservoirs. The entropy generation equation for the two-stage cryogenic system is given by the sum of Eqs. (9) and (10). Substitution of Eqs. (1), (2), (6), and (7) and the subsequent simplification of the resulting expression eventually yields

$$\dot{S}_{gen,TTL} = \frac{\dot{W}_1 + \dot{W}_2 + \dot{Q}_{g,M} + \dot{Q}_{g,L}}{T_H}. \tag{11}$$

Cryocooler efficiency affects the entropy generation rate through the input power and the related heat of rejection terms. The rate of entropy generation would at first glance appear to be unaffected by the parasitic losses since they do not appear in the equation. However, larger parasitic heat loads require higher cryocooler input power, which in turn increases the magnitude of the entropy generation rate. Similarly, heat leaks from the first stage to the second stage result in a larger total cryocooler input power, hence a larger total entropy generation rate, because cryocooler efficiencies decrease as the temperature delta over which the heat must be pumped is increased.

The optimum thermodynamic operating point occurs when the rate of entropy generation is minimized, and the sensitivity of the entropy generation rate to any variable in the right-hand-side of the equation is determined by taking the derivatives of the function with respect to the variable(s) of interest, say x. The optimum value of x is therefore determined by satisfying the following relationships:

$$\frac{\partial \dot{S}_{gen,TTL}}{\partial x} = 0, \tag{12}$$

$$\frac{\partial^2 \dot{S}_{gen,TTL}}{\partial x^2} > 0. \tag{13}$$

The same approach can be used for multi-variable optimization by developing and solving a set of simultaneous equations from the appropriate partial derivatives.

APPLICATION OF TECHNIQUE

This example illustrates the optimization technique applied to a cryogenic spacecraft payload with either single or multi-stage cryocoolers. Consider the system illustrated in Figure 2, which contains a subset of the thermal processes from the generalized discussion. For the purposes of the example, assume the geometry is fixed, the temperature extremes are fixed at $T_H = 300\,\mathrm{K}$ and $T_L = 100\,\mathrm{K}$, and the goal is to determine the optimum intermediate temperature, T_M. Convection losses are zero. The support conduction and MLI radiative paths are in parallel and can be optimized independently as shown by other authors. However, the optimized heat intercept temperature for the support is generally different than the corresponding optimized shield temperature for the MLI. For practical applications, a single cold shield serves as both the support intercept and the radiation shield so that a single 2-stage cooler can satisfy the cryogenic cooling requirements. Hence, this optimization exercise is performed combining conduction and radiation effects.

The optimum shield temperature is determined from Eqs. (12) and (13), the entropy minimization equations, where $x = T_M$. Combining Eqs. (11) and (12) and dropping the heat generation terms that do not apply to this example provides the optimization equation:

$$\frac{\partial \dot{S}_{gen,TTL}}{\partial T_M} = \frac{1}{T_H}\frac{\partial}{\partial T_M}\left\{\dot{W}_1 + \dot{W}_2\right\}. \tag{14}$$

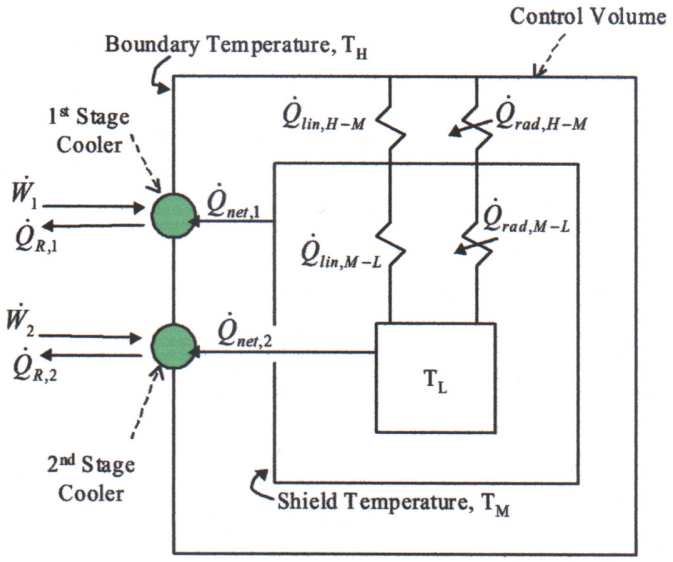

FIGURE 2. Thermal schematic of two-stage cryogenic system showing the intercept of a portion of the parasitic load at the intermediate temperature level.

Cryocooler efficiency is commonly expressed as the specific power, $\dot{W}_{sp}$, which is defined by the expression

$$\dot{W} = \dot{W}_{sp} \times \dot{Q}_{net}. \tag{15}$$

Substituting for the work terms using Eq. (15) into Eq. (16) yields the expression

$$\frac{\partial \dot{S}_{gen,TTL}}{\partial T_M} = \frac{1}{T_H}\frac{\partial}{\partial T_M}\left\{\dot{W}_{sp,1}\left(\dot{Q}_{p,HM} - \dot{Q}_{p,ML}\right) + \dot{W}_{sp,2}\left(\dot{Q}_{p,ML}\right)\right\}. \tag{16}$$

The solution of Eq. (16) now reduces to variable substitution and the systematic application of the Chain Rule to insure that all functional dependencies on the variable T_M are considered. For example, the variables k and ε^* affect the optimum shield temperature and have a functional dependency on the shield temperature as shown by the expression

$$\dot{Q}_{p,HM} = \dot{Q}_{lin,H-M} + \dot{Q}_{rad,H-M} = \frac{k(T)A_{c,H}}{L_H}\left(T_H - T_M\right) + \sigma\varepsilon^*(T)A_{s,H}\left(T_H^4 - T_M^4\right), \tag{17}$$

where k, $A_{c,H}$, and L_H are the thermal conductivity, cross sectional area, and length of the support from T_H to T_M, σ is the Stefan-Boltzmann constant, and $A_{s,H}$ is the surface area of the MLI blanket that resides between T_H and T_M. Therefore, the evaluation of Eq. (16) necessarily entails the differentiation of k, ε^* and any other system variables with a functional dependence on the shield temperature, in particular, the specific power of the first stage cryocooler and all of the parasitic loads at both stages.

The cryocooler lost power is obtained by multiplying Eq. (9) by the system reference temperature, T_H. For the case of Carnot cryocoolers, the entropy generation and lost power in the cryocoolers is zero, and the only entropy generation in the total system is that due to heat transfer within the cooled subsystem. The minimum, or Carnot, cryocooler power for a given payload design is therefore given by the product of T_H and Eq. (10). The total power for a real cryogenic system is given by the sum of the Carnot power and the lost power, or directly by the product of T_H and Eq. (11). In summary,

$$\text{Lost Cryocooler Power:} \quad \dot{W}_{lost} = T_H \dot{S}_{gen,cooler}, \tag{18}$$

$$\text{Carnot Cryocooler Power:} \quad \dot{W}_c = T_H \dot{S}_{gen,subsys}, \tag{19}$$

$$\text{Total Cryocooler Power:} \quad \dot{W}_{TTL} = T_H \dot{S}_{gen,TTL} = \dot{W}_{lost} + \dot{W}_c . \tag{20}$$

CONSIDERATION OF NON-IDEAL CRYOCOOLER PERFORMANCE

The thermodynamic efficiency of an ideal, reversible cryocooler operating between temperature reservoirs T_H and T_L is equal to the Carnot efficiency, defined by the expression $\beta_c = T_L/(T_H - T_L)$. The Carnot specific power is simply the inverse of the Carnot efficiency. Analyses based upon the assumption of ideal cryocooler efficiencies can be misleading because of the dramatic departure of the real (*e.g.* Stirling, pulse tube, etc.) cryocooler efficiencies from Carnot, particularly as the refrigeration temperature decreases. Figure 3 contains a plot of specific power versus cold tip temperature based upon an extensive review of measured performance data for space-borne cryocoolers from U.S. and European manufacturers. The data span the temperature range of 4 K to 150 K for rejection temperatures between 295 K and 300 K. Most of the cryocoolers represented are single-stage machines, though a few are multi-stage machines in which only the coldest stage was thermally loaded. The specific power data were successfully fit to a power-law relationship of the form $C_0 T^{-n}$ with $C_0 = 3.7709\text{E+}05$, $n = 2.2516$. For the purposes of this example, it was assumed that the correlation could be extrapolated to refrigeration temperatures up to 200 K.

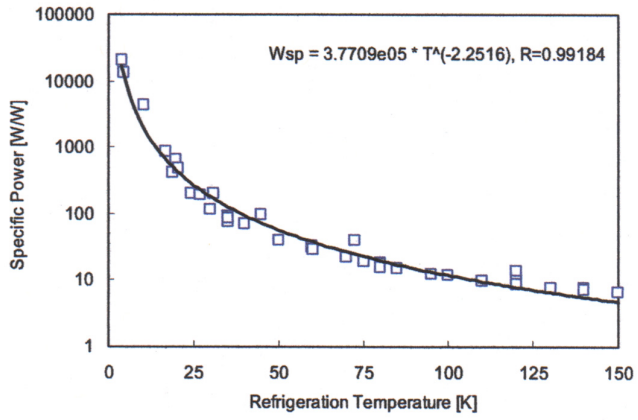

FIGURE 3. Space cryocooler specific power vs. temperature data. Compilation of data from numerous manufacturers successfully curve fit to the power law function shown [ref 7,8,9,10,11].

The derivation of Eq. (16) is general with respect to the cryocooler configuration, that is, whether the system has two single-stage or a single two-stage cryocooler. In the case of a two-stage cryocooler, the mathematics are more complicated because of the dependency of each stage efficiency on the temperature of every stage, not just the particular stage at which the efficiency is being calculated. For example, in the case of two independent cryocoolers, $\beta_1 = f(T_H, T_M)$ and $\beta_2 = g(T_H, T_L)$, but for a two-stage cryocooler in which there is thermodynamic communication between temperature stages within the cryocooler itself, $\beta_1 = f(T_H, T_M, T_L)$ and $\beta_2 = g(T_H, T_M, T_L)$. From a mathematical perspective, the broader functional dependency of these variables results in more terms when the $\dot{S}_{gen}$ function is differentiated. From a practical perspective, there is much less data available from two-stage cryocoolers to construct curve fits of the type illustrated in Fig. 3, and the data are less given to simple curve fits because of the more complicated functional relationships. Kirkconnell and Price describe a methodology for minimizing the entropy generation rate in multi-stage cryocoolers from the perspective of the cryocooler designer, that is, when the governing equations for the thermodynamic interactions between the stages are known [12]. The methodology described therein can be combined with that provided in this paper to develop a set of governing equations describing the physics of both the cryocooler and the cryogenic system. However, these governing equations are unique to every cryocooler, so such an analysis presumes that the cryocooler has already been selected. The present effort assumes the more general case where the cryogenic system designer relies upon published cryocooler performance data. The additional simplification made is that the efficiency at each stage, and hence the total cryocooler input power, is independent of the cryocooler configuration (single-stage vs. multi-stage). One would expect the numerical value of the results to shift when the configuration-specific efficiencies are taken into account, but the fundamental optimization approach is the same.

MULTILAYER INSULATION (MLI) FOR CRYOGENIC APPLICATIONS

For more than 30 years, the development of MLI blankets for cryogenic applications has been driven by the need to improve performance while reducing design complexity and total implementation cost. This has resulted in extensive testing of layer configurations and materials by various laboratories. Testing has been performed on both ideal configurations such as flat plate calorimeters and more practical systems involving dewars, propulsion tanks, spacecraft and payloads for IR systems. Results of these tests have shown a large variation in thermal performance by as much as 2 to 10 times or more due to a variety of factors. These factors have been reported in the literature and generally consist of effects from discontinuities at edges or seams, vent holes, support or cable penetrations, layer density or contour compression, and effects from stitches and joints. Other effects involve changes of metallized layer emittance with temperature and the dominance of conduction effects at low temperature. Some reported correlations and attempts to model these effects have taken various forms generally based on combinations of conductance and radiation terms with/without temperature dependent coefficients. These correlations have been made with varying layer densities, penetrations, and blanket areas to derive empirical values for effective thermal conductivity and effective emittance, typically designated ε^*.

In the example considered here, a range of blanket performance is considered to illustrate how the selected ε^* correlation equations impact the heat loads and, ultimately, the optimum shield temperature, T_M. Data were taken from two sources that bracket a fairly broad range of MLI effectiveness. Results obtained using ε^* values based upon

Lockheed Martin (LHM) data for an idealized tank calorimeter [13] are compared to those obtained using ε^* correlations derived from a Deutsche Aerospace (DA) compilation of data for more realistic spacecraft blankets [14]. In the example to follow, the cold and hot boundary temperatures are known, 100 K and 300 K, so the LHM and DA data were reduced in terms of a single independent variable, T_M, to simplify the calculations. This allowed for straightforward power law correlations of the form $\varepsilon^* = C_L / T_M^{aL}$ and $\varepsilon^* = C_H / T_M^{aH}$ for the cold and hot side blankets, respectively. For the LHM data, $C_L = 0.0871$, $aL = 0.664$, $C_H = 0.00611$, and $aH = 0.247$, and for the DA data, $C_L = 17.74$, $aL = 1.215$, $C_H = 0.0713$, and $aH = 0.305$. The reader is directed to references 13 and 14 for details on the experimental measurements upon which the curve fits were based.

RESULTS

Results were obtained for a sample problem with temperature extremes of 100 K and 300 K assuming thermoplastic supports with $A_c/L = 0.1$ m on both sides of the thermal shield and $A_{s,H} = 0.46$ m^2 and $A_{s,L} = 0.35$ m^2 for the hot and cold side blanket surface areas, respectively. Linear temperature dependence of the support thermal conductivity was assumed ($k = 0.12$ W/m/K @ 100 K, 0.24 W/m/K @ 300 K). A spreadsheet model was built that calculates the work terms and derivatives for a range of T_M values. The results for the Carnot power and real (total) power using the DA MLI data are shown in Figure 4b. Note that the optimum shield temperature for the Carnot case is about 10 K higher than that for the real case. Plots of the partial derivatives, shown in Figure 4a, demonstrate these same characteristics of the power curves. The zero crossings and the positive slopes of the curves at those cross points are simply a graphical restatement of the minimums visually identifiable in Fig. 4b. Solution methods employing the use of the derivative expressions are much more efficient for identifying the optimum operating point for multi-variable optimization problems because one can simply set up and solve a system of simultaneous equations to identify the optimum combination of variables. An example would be the simultaneous determination of the optimum shield temperature and intercept location along a conduction support of fixed length. The authors plan to present the results of a multi-variable optimization study in a future article.

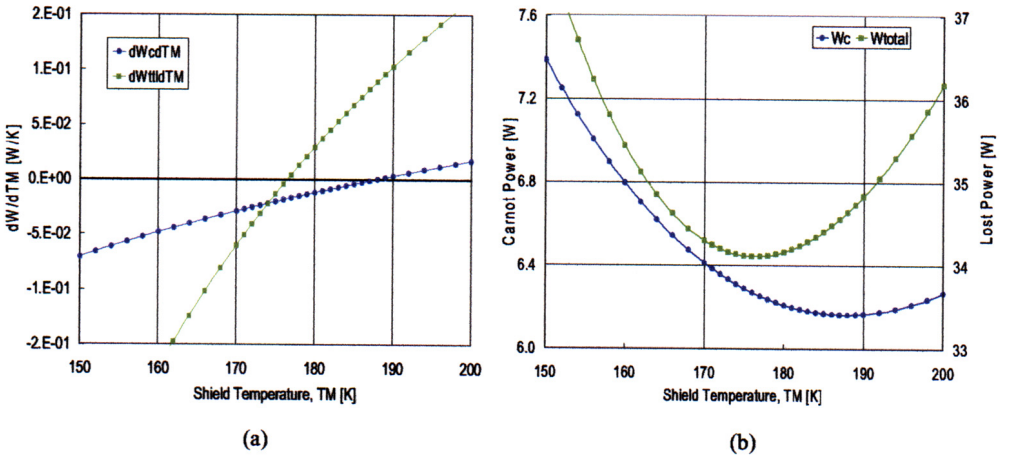

FIGURE 4. Optimization curves for sample problem using DA MLI data. Carnot and real cryocooler results shown. a) Partial derivatives of Carnot power and lost power. b) Power vs. shield temperature.

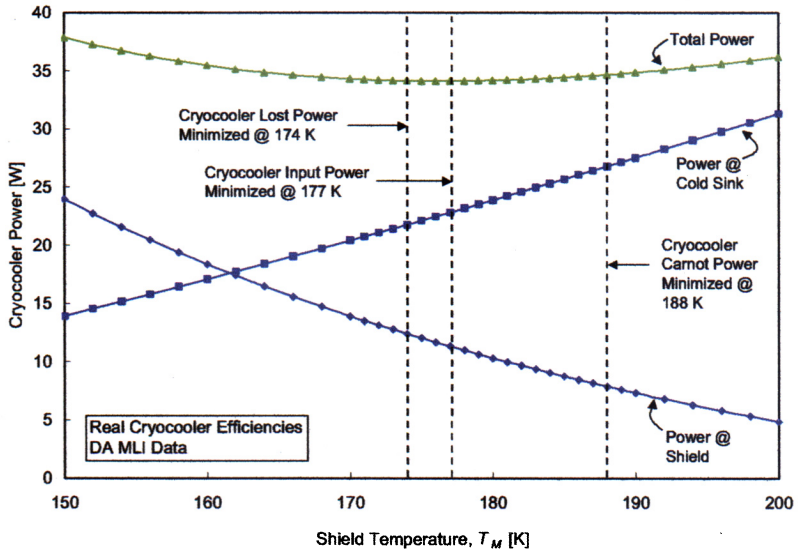

FIGURE 5. Cryocooler power allocation for real cryocoolers using DA MLI data. 3 K difference between shield temperature of minimum cryocooler lost power and that of minimum entropy generation.

The distribution between 1st and 2nd stage cryocooler input power as a function of shield temperature for the real cryocooler case using DA MLI data is provided in Figure 5. Also shown are the shield temperatures corresponding to minimum total, lost, and Carnot cryocooler power. The optimum system-level shield temperature (177 K) lies between the optimum cryocooler shield temperature (174 K) and optimum payload shield temperature (188 K), which is given by the location of minimum Carnot power per Eq. (19).

Results were also obtained using the effective emissivity correlations derived from the LHM tank calorimeter MLI data, which yields ε^* values about 1/10th of the DA data. The radiation terms are only about 5 to 10% of the magnitude of the conduction terms using the small ε^* values calculated from the flat plate correlations (0.001 to 0.003). By comparison, the DA correlations yield ε^* values between 0.01 and 0.04, which is more typical of what one might expect for a system-level blanket with seams and penetrations, and the resultant conduction and radiation terms are roughly equal. The radiation parasitic loss terms are governed by fourth order temperature dependence, so the total decrease in first stage load relative to second stage load is much greater in going from high ε^* values to low ε^* values. Therefore, the impact of operating the shield at a lower temperature on first stage cryocooler power is much less, but the benefit of reduced second stage load is almost fully realized because the parasitic loss is conduction dominated. The result is lower optimum shield temperatures for the idealized LHM blanket case.

Table 1. Summary of Results at Optimum Shield Temperatures

	Optimum T_M [K]	1st Stage Cooler Power [W]	2nd Stage Cooler Power [W]	Total Cooler Power [W]	Lost Cooler Power [W]
Carnot Cryocoolers					
-DA MLI Data	187.8	1.653	4.510	6.164	0.000
-LHM MLI Data	180.1	0.959	2.924	3.883	0.000
Real Cryocoolers					
-DA MLI Data	177.0	11.298	22.809	34.107	27.854
-LHM MLI Data	170.3	6.639	14.723	21.363	17.608

Table 2. Results Obtained at Minimum Cryocooler Lost Power Operating Point

	T_M @ Minimum Lost Power [K]	1st Stage Cooler Power [W]	2nd Stage Cooler Power [W]	Total Cooler Power [W]	Lost Cooler Power [W]
Real Cryocoolers					
-DA MLI Data	174.0	12.354	21.779	34.133	27.819
-LHM MLI Data	167.6	7.280	14.273	21.553	17.587

The power results at the optimum shield temperatures for each of the four configurations are summarized in Table 1, and Table 2 shows the power results at the shield temperature corresponding to minimum cryocooler lost power. Note that the total cooler power values are slightly higher in Table 2, consistent with the fact that the rate of entropy generation is minimized at the total system level, not the cooler level, to determine the proper optimum shield temperature. For this particular example and many other typical applications, the shield temperatures that yield minimum cryocooler lost power and minimum system-level entropy generation are close.

CONCLUSION

The proper application of second law thermodynamic methods facilitates the optimization and characterization of multi-stage cryogenic systems. By identifying where entropy is being generated, by what modes, and the relative amount of the lost power and Carnot power terms, the thermal designer can properly focus his efforts on the aspects of the design most amenable to and in need of improvement. Optimization studies based upon idealized efficiencies, such as the use of Carnot efficiencies or theoretically optimum MLI blanket ε^* values, can yield incorrect results and, therefore, inefficient thermal systems. This paper has shown that actual hardware characteristics need to be used.

REFERENCES

1. Bejan, A. and Smith, J.L., Jr., "Thermodynamic Optimization of Mechanical Supports for Cryogenic Apparatus," *Cryogenics* **14** (1974).
2. Bejan, A., "The Concept of Irreversibility in Heat Exchanger Design: Counterflow Heat Exchangers for Gas-to-Gas Applications," *Journal of Heat Transfer* **99** (1977).
3. Hilal, M.A. and Boom, R.W., "Optimization of Mechanical Supports for Large Superconductive Magnets," *Adv. in Cryo. Eng.* **22** (1977).
4. Seol, S.Y., Chyu, M.-C., Kuzay, T.M., and Hull, J.R., "Minimization of Refrigeration Power Requirements for Mechanical Supports in Cryogenic Systems," *Cryogenics* **22** (1992).
5. Chang, H.-M and Van Sciver, S.W., "Thermodynamic Optimization of Conduction-Cooled HTS Current Leads," *Cryogenics* **38** (1998).
6. Bejan, A., Advanced Engineering Thermodynamics, John Wiley & Sons, New York (1988), pp. 50-67.
7. Price, K.D., Raytheon, private communication.
8. Tward, E., TRW, private communication.
9. Nast, T.C., Lockheed Martin, private communication.
10. Gully, W.J., Ball Aerospace, private communication.
11. Baker, G., Matra Marconi Space, private communication.
12. Kirkconnell, C.S. and Price, K.D., "Thermodynamic Optimization of Multi-Stage Cryocoolers," *Cryocoolers 11*, Kluwer Academic/Plenum Publishers, New York (2001), pp. 69-78.
13. Spradley, I.E., Nast, T.C., and Frank, D.J., "Experimental Studies of MLI Systems at Very Low Boundary Temperatures," *Adv. in Cryo. Eng.* **35** (1990).
14. Doenecke, J., "Survey and Evaluation on Multilayer Insulation Heat Transfer Measurements," *SAE Technical Paper 932117*, (1993).